CHINESE JOURNAL OF PHYSICS VOL. 52, NO. 1-I February 2014

Physical Properties of TCO - ZnO Thin Films Sputtered from a Powder Target

F. Chaabouni,* J. B. Belgacem, and M. Abaab

Ecole Nationale d'ingénieurs de Tunis, 99/UR/11-35,
Laboratoire de Photovoltaïque et Matériaux Semiconducteurs, 1002, Tunis, Tunisie
(Received May 21, 2013)

Zinc oxide (ZnO) thin films were deposited by RF magnetron sputtering employing a low cost ZnO powder target. In this paper, the effect of the deposition time and the argon pressure on the structural, morphological, electrical, and optical properties of ZnO thin films are described. X-ray diffraction (XRD) results indicated that all the thin films have a preferential c-axis orientation and that the peak position of the (002) plane was shifted to the high 2θ values as both the deposition time and argon pressure increased. The crystallite size was found to be in the nano range of 20–27 nm, showing that the films are nanostructured in nature. The optical transmittance in the visible region was desirably high ($> 85\%$), the refractive index reached 2.28, and the films demonstrated an optical band gap of about 3.3 eV. The films' resistivity was in the range of 7×10^{-3} to 8×10^{-2} Ω·cm. The obtained ZnO films demonstrated the good properties required for transparent conducting oxide applications, namely an enhanced transmission, a reduced average crystallite size, and a reduced resistivity without any doping or post-deposition annealing. Among all of the zinc oxide films obtained in this study, films grown at 1.2 Pa exhibited the best properties for TCO applications: a refractive index of 1.98, an internal stress of 0.5 GPa, and a resistivity of 2.3×10^{-2} Ω·cm. The results demonstrate that magnetron sputtering from powder targets is a versatile technique for the deposition of high quality transparent conductive ZnO films.

DOI: 10.6122/CJP.52.272 PACS numbers: 81.15.Cd, 73.61.Ga, 78.66.Hf

I. INTRODUCTION

ZnO is a II–VI compound semiconductor with a wide direct band gap of 3.37 eV at room temperature. It is abundant and non-toxic; it has relatively high thermal and chemical stability, large mechanical strength, and large piezoelectric coefficients. It is a versatile semiconductor material, which has attracted attention for its wide range of applications, such as solar cells [1], light emitting diodes [2], UV laser [3], electrical and acoustic devices [4], and chemical sensors [5, 6].

Among all the TCOs, zinc oxide has emerged as one of the most promising materials, due to its unique combined electrical and optical properties.

Low resistive and highly transparent ZnO thin films are required for solar cell and many other optoelectronic applications. But pure ZnO thin films have a high resistivity

*Electronic address: fchaabouni@yahoo.fr

due to their stoichiometric nature, which could not produce large number of free charge carriers. In order to enhance the conductivity of ZnO thin films, they can be doped with a wide variety of elements of group I, such as Li, and of groups III or V, such as Al, Ga, In, N, P, As, Sb, etc. [2, 7, 8]. Several deposition techniques have been used to prepare the thin ZnO films, such as plasma enhanced chemical vapour deposition (PECVD) [9], pulsed laser deposition (PLD) [2, 7], evaporation, the sol–gel method [5], spray pyrolysis [1], molecular beam epitaxy (MBE) [10], and sputtering [4, 8].

Compared to other techniques, sputtering offers several advantages in producing thin films suitable for the solar applications, such as safety, simplicity, non-toxic gas emissions, its potential for low temperature processing with a high deposition rate, easiness to expand to large area films, the composition of the grown films is quite close to that of the target, the surface of the films is very smooth, and the film thickness can be easily controlled by adjusting the deposition time.

Most of investigations used hot pressed or sintered ceramic ZnO as a target material in sputtering, which may have a tendency to crack unless sputtered at low powers, restricting thus the deposition rate. Although some researchers have grown ZnO films at very low temperatures, such as room temperature, the effects of radio frequency (RF) power using a powder target on the structural, electrical, and optical characteristics of ZnO thin films have not been sufficiently investigated.

In this article, we report on the investigation of the effect of deposition time and argon pressure on ZnO thin films grown by RF magnetron sputtering using a powder target. This low cost technique does not need target processing, and it can be extended to multi-dopant target compositions.

In the present study, the undoped ZnO films grown at room temperature with a powder target show TCO properties.

II. EXPERIMENTAL PROCEDURE

The ZnO films were deposited on glass substrates by an RF magnetron system using a powder target (99.99% in purity) at room temperature with an RF power of 150 W. The powder was evenly distributed across the surface of a copper backing plate on the magnetron to form a target. The powder was lightly tamped down to produce a uniform thickness and surface to target distance. No further processes were involved in target production. The powder is loosely packed, so target cracking issues are avoided, and the target composition can be readily varied. Furthermore, the starting materials are relatively cheap, and, since the powder can be simply redistributed across the target, no permanent race track is formed, and the material utilization is very high compared to a solid target. This is a highly flexible deposition technique, which has been successfully used to deposit a range of TCO and other coating materials, including doped zinc oxides [11, 12]. The chamber was evacuated to a pressure of 5×10^{-5} Pa. The substrate holder was placed at 65 mm away from the target. The deposition time was varied to 2, 4, and 5 h with a fixed argon pressure of 0.6 Pa, and the argon pressure was varied to 0.3, 0.6, 0.9, and 1.2 Pa with

a deposition time of 4 h. The substrates were not intentionally heated during deposition.

The obtained ZnO films were characterized using X-ray diffraction (PANalytical X'Pert Pro, Philips Co, Ltd) with CuK_α radiation ($\lambda = 0.15406$ nm). Surface morphology was observed using an Atomic Force Microscopy (AFM, Nanoscope IIIa Veeco type dimension 3100).

The optical properties of the films were measured at normal incidence in the wavelength range, from 300 to 1800 nm, using a double-beam UV-VIS-NIR spectrophotometer (Shimadzu).

AC electrical properties were characterized by impedance spectroscopy (impedancemeter, HP 4192 A).

III. RESULTS AND DISCUSSIONS

III-1. Structural properties

The XRD patterns of the ZnO films grown on glass substrates are shown in Fig. 1. The spectra show that all the films have only one peak at 2θ near 34.25 to 34.4°. This peak is identified as the wurtzite (002) peak, suggesting that all samples are polycrystalline with a preferential orientation along the c axis perpendicular to the substrate plane. This confirms that the films grow with a hexagonal wurtzite structure.

Moreover, the preferential (002) peak intensity increases and the peak broadening decreases with increasing argon pressure and the deposition time, which reveals an enhancement in the crystallinity of the films. This may be associated with a decrease in lattice strain and a more periodic arrangement of the crystals or an increase in the film thickness. It has been shown that at the initial deposition, the crystallinity was poor, as indicated by a low (002) peak intensity, and became stronger as the film thickness increased. Gardeniers *et al.* [13] and Knuyt *et al.* [14] reported that the film tends to lower its surface energy during deposition, which is achieved by diffusion within a thin surface layer of atoms from a particular crystallite to one having a lower surface energy. As a result of this process, the lower-surface-energy grain will become larger as the film thickness increases, while the orientation distribution at the surface evolves towards one corresponding to the crystallographic direction of lowest surface energy.

The average grain size (L) was estimated by Sherrer's formula [15]:

$$\mathrm{L} = \frac{0.9\lambda}{\cos\theta_0 \Delta(2\theta)}, \tag{1}$$

where λ is the X-ray wavelength of the Cu Kα radiation (k = 1.5418 Å), θ_0 is the Bragg angle, and $\Delta(2\theta)$ is the experimental full-width at half-maximum (FWHM) of the respective diffraction peak measured in radians.

The grain size slightly increases from 23.6 to 27 nm with an increase in the argon pressure, as found by Subramanyam *et al.* for ZnO films grown by sputtering with different argon pressures. The grain size also increases with an increase of the deposition time from 19 to 27.5 nm, suggesting an enhancement in the degree of crystallinity of the films. Chang

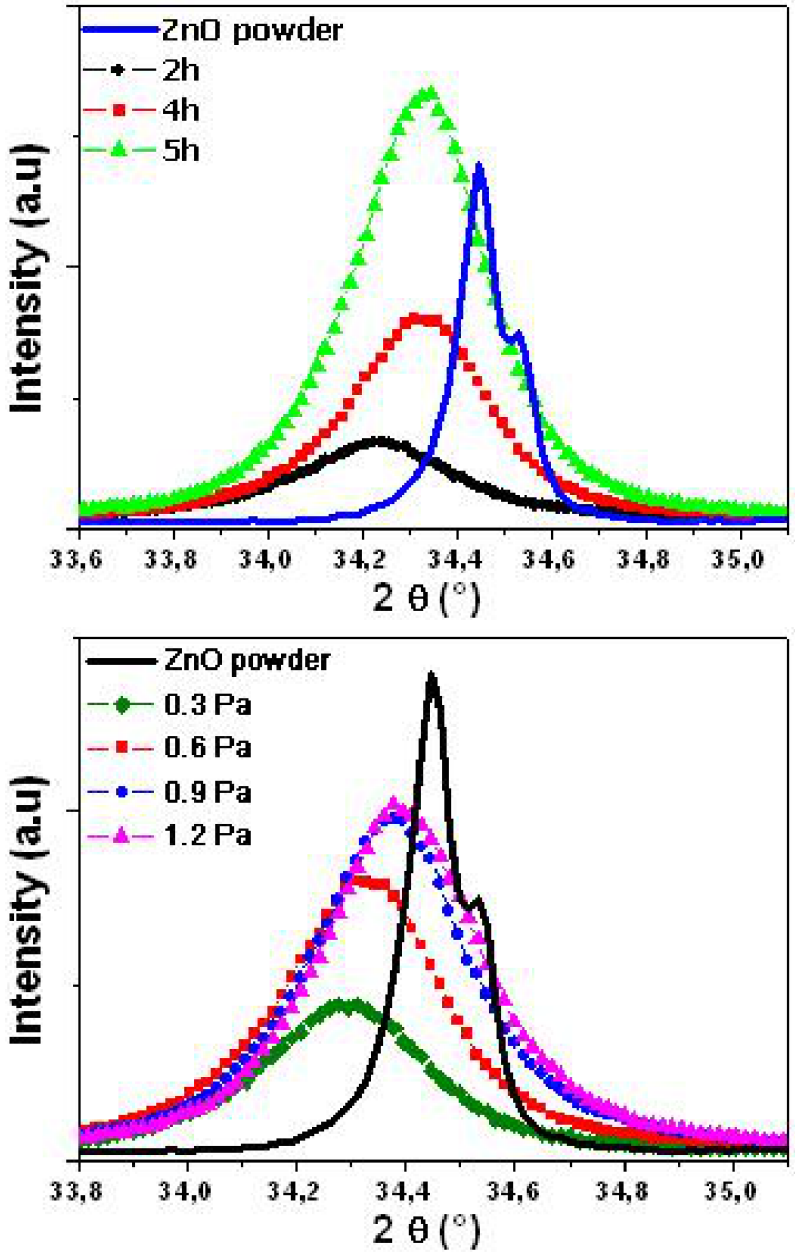

FIG. 1: XRD spectra for ZnO films deposited with (a) different deposition times, and (b) different argon pressures.

et al. [16] stated that at the initial stage of deposition, a large amount of small grains is distributed at arbitrary sites, and in the following growth the grains become larger, and finally large grains with columnar structure are formed.

The peak position of the (002) plane was shifted to the high 2θ value with an increase of the deposition time and argon pressure, as shown in Figure 2, approaching the 2θ value of the ZnO powder used. The deviation of the (002) peak position can be attributed to the stress generated at the ZnO film/glass substrate interface.

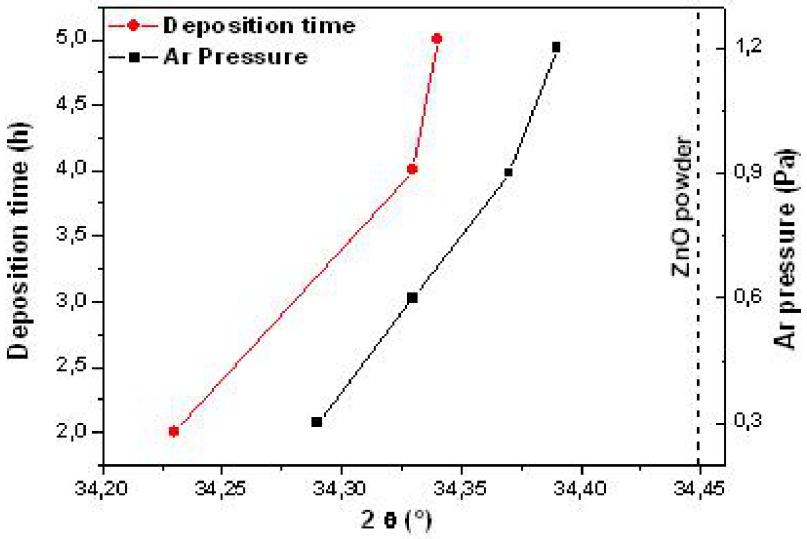

FIG. 2: Variation of the 2θ angle of the (002) peak with deposition time and argon pressure.

The microstructure and thus the intrinsic stresses in vacuum-deposited coatings are sensitive to the deposition conditions. Residual stresses always develop in the films, because the film and the substrate differ in atomic distance, thermal expansion coefficient, and cooling conditions. Large residual stresses may cause micro-cracks in the film or peeling of the film from the substrate. Therefore, control of the residual stress is essential for synthesizing mechanically stable ZnO films.

The ZnO (002) diffraction peak is seen at 2θ from 34.23 to 34.34° as the deposition time increases, and is seen at 2θ from 34.29 to 34.39° as the argon pressure increases. For films grown at an Ar pressure of 1.2 Pa, the lattice constant is closer to that of the ZnO powder used (34.45°). The relaxation of the strain with deposition time and argon pressure increase causes such a shift in the peak position. We found that the deposition time and the argon pressure recover the 2θ angle, and hence repair the lattice constant.

The calculation of the mean film stress σ_{film} is based on the biaxial strain model. The strain e_{zz} in the c axis, i.e., perpendicular to the substrate surface, was measured by XRD. To derive the film stress parallel to the film surface, the following formula is used, which is valid for a hexagonal lattice [17]:

$$\sigma_{\text{film}} = \left(2C_{13} - \frac{\left((C_{11} + C_{12}) \times C_{33}^{\text{film}} \right)}{C_{13}} \right) \times e_{zz}, \tag{2}$$

with $C_{33}^{film} = \frac{0.99 \times C_{33}}{(1-e_{zz})^4}$ [18] and $e_{zz} = \frac{c_{film} - c_{bulk}}{c_{bulk}}$, $C_{11} = 209.7$ GPa, $C_{12} = 121.1$ GPa, $C_{13} = 105.1$ GPa, and $C_{33} = 210.9$ GPa are the elastic stiffness constants of the bulk ZnO [19], c_{bulk} and c_{film} are the constants of the strain-free bulk ZnO and the lattice constant of ZnO film, respectively.

The values of the internal stress estimated (< 2.5 GPa) are relatively low and acceptable, proving the good quality of the grown films, especially as they were grown at ambient temperature and didn't have any post deposition annealing. Moreover, the crystallinity enhancement obtained with an increase of the deposition time is accompanied with a remarkable decrease of the stress from 2.5 to 1 GPa, leading to the reduction of lattice imperfections.

Films grown at an argon pressure of 1.2 Pa show the lowest value of lattice strain of 0.5 GPa.

It is known that the sputtering pressure has a strong influence on the film stress [20]. At low pressure, the sputtered films exhibit compressive stress, which decreases with increasing pressure, leading to a tensile stress for very high argon pressure.

The compressive stresses decreased with an increase of the pressure. This is similar to ZnO thin films grown by Hinze *et al.* [21], with a working pressure from 0.13 to 2.9 Pa.

III-2. Morphological properties

Fig. 3 a–c, d–f shows the AFM images of ZnO films deposited for different deposition times and different argon pressures, respectively.

AFM images show homogenous, dense, and good quality film surfaces. The films exhibit closely packed columnar morphology with uniform texture and size distributions. For some samples, we notice the presence of some pores reducing the density of the films.

The roughness increases slightly with the deposition time varying from 6.5 to 13 nm. These film surface morphologies have a potential application in enhanced light trapping, particularly in photovoltaics.

The porosity of the films increases with argon pressure, especially for films grown at 1.2 Pa, suggesting that an increase of the deposition pressure leads to porous films. Indeed, AFM images show microstructural evolution from a dense state ("T zone" type) to a porous state ("Zone 1" type), as stated in Thornton model [20] for the sputtered films, as the deposition pressure increases from 0.3 to 1.2 Pa. These results are confirmed by the decrease of the refraction indexes of the films.

III-3. Optical properties

The optical transmittance of the ZnO films deposited at various deposition times and argon pressures are plotted in Fig. 4. All the transmission spectra show interference fringe patterns characteristic of fairly uniform thickness and quite homogenous layers, in accordance with the study of morphological analysis. The average transmittance in the visible range was over 85%, indicating a good transparency of the films. For most optical applications, a high transmittance in the visible range is very important.

Fig. 4 shows a sharp fall of the transmittance at the band edge. A fair red shift of the

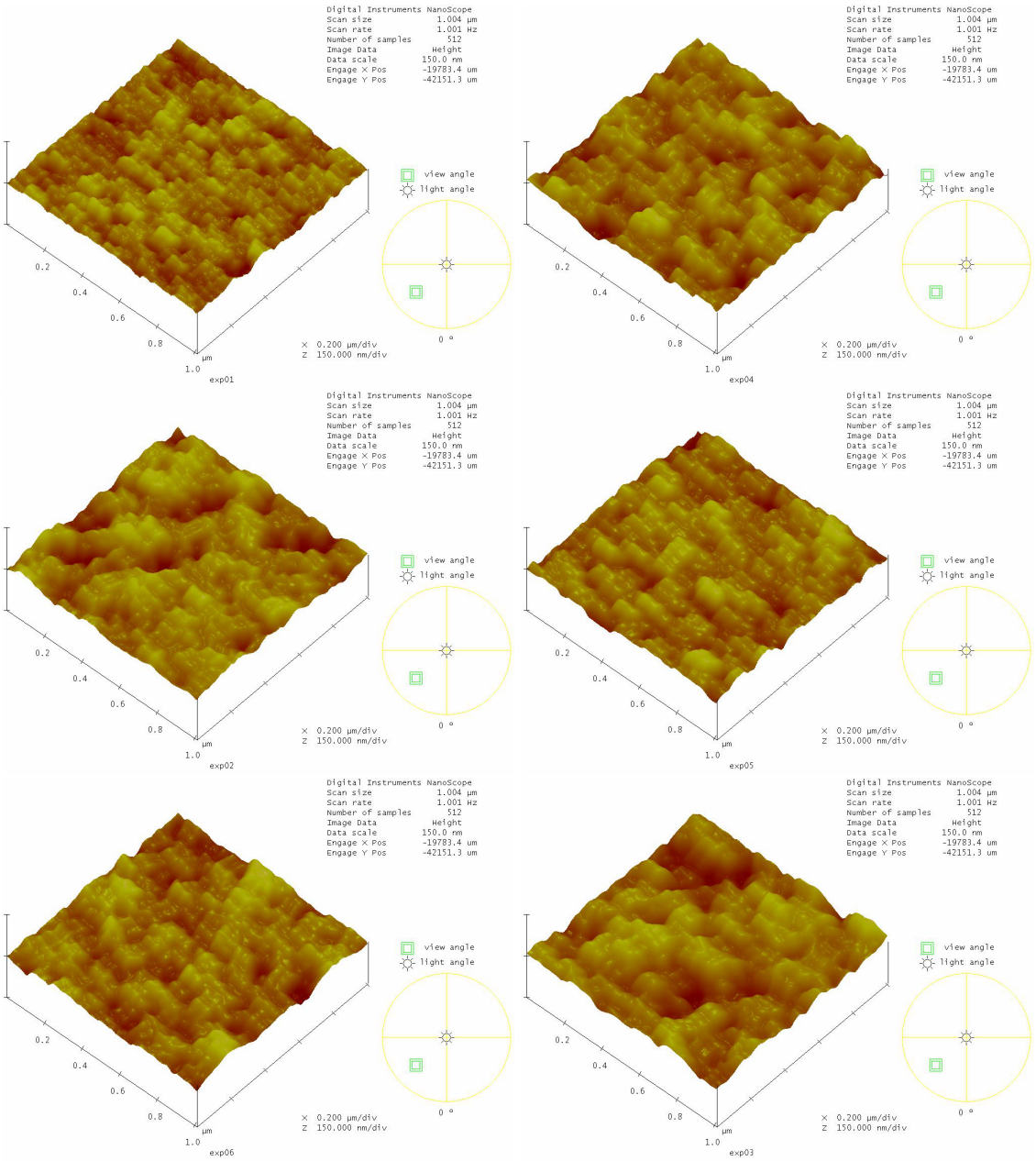

FIG. 3: AFM images of ZnO films deposited with different deposition time (a) 2 h, (b) 4 h, (c) 5 h and different argon pressures (d) 0.3 Pa, (e) 0.9 Pa, (f) 1.2 Pa.

absorption edge is also noticed in the transmission spectra for films deposited at different deposition times, as shown in Fig. 1a.

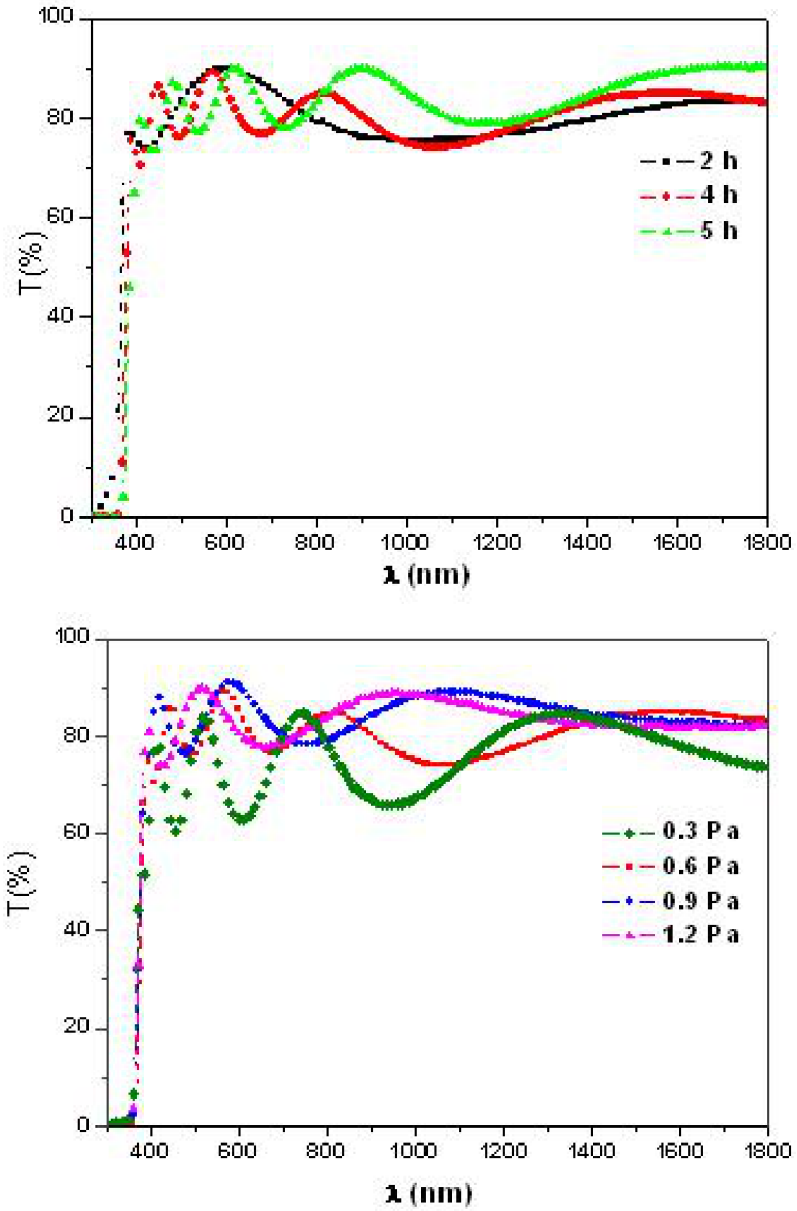

FIG. 4: Transmission spectra for ZnO films deposited with (a) different deposition time, and (b) different argon pressures.

The absorption coefficient (α) near absorption edge is calculated by

$$\alpha = \frac{1}{\mathrm{d}} \mathrm{Ln} \left(\frac{(1-\mathrm{R})^2}{\mathrm{T}} \right), \tag{3}$$

where d is the film thickness, T and R are the film transmission and reflectance, respectively.

The absorption coefficient spectra are shown in Figure 5. The sharp fall of the absorption at the band edge is an identification of the good crystallinity of the films. This result is very important because we know that the spectral dependence of the absorption coefficient affects the solar conversion efficiency.

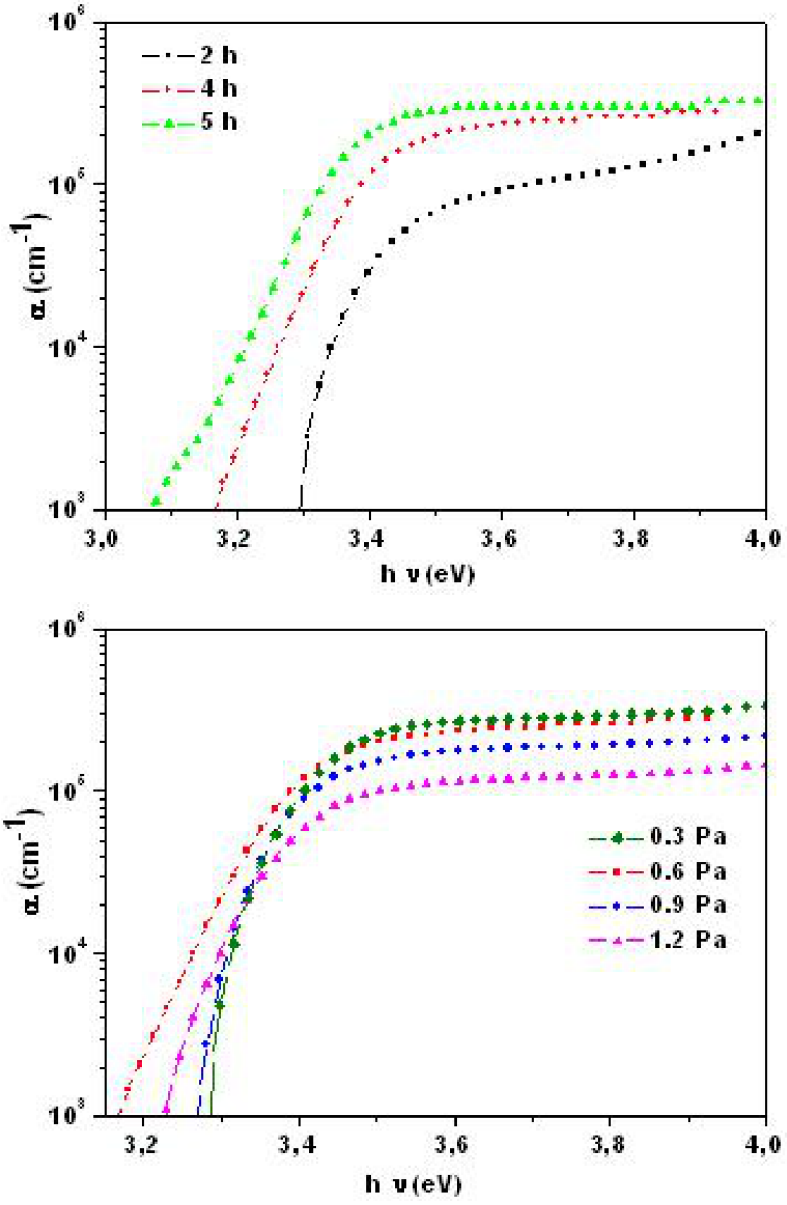

FIG. 5: Absorption coefficient for ZnO films deposited with (a) different deposition time, and (b) different argon pressures.

It can be seen that all the films have a relatively high absorption of the order of 10^5

cm^{-1}. The absorption coefficient increases with the deposition time up to 3×10^5 cm^{-1} in the UV (A and B) region, and decreases with argon pressure up to a value of 1.5×10^5 cm^{-1}. This indicates that these films absorb well UV radiation and can be used as anti UV coating films.

The value of the optical band gap E_g was determined by measuring the optical transmission and reflection spectra and using the Tauc plot [22]:

$$(\alpha h\nu)^2 = A(h\nu - E_g), \tag{4}$$

where A is a constant known as the band edge sharpness, and $h\nu$ is the photon energy. The direct band gap E_g is determined by extrapolating the linear part of the $(\alpha h\nu)^2$ vs. $h\nu$ curve at high absorption data ($\alpha > 10^4$ cm^{-1}) to the intercept of the horizontal photon energy axis.

The linear dependence of $(\alpha h\nu)^2$ on $h\nu$ at higher photon energies indicates that the grown ZnO films have essentially direct-transition-type semiconductors. Extrapolation of the linear portions of $(\alpha h\nu)^2$ to zero gave the value of E_g.

Fig. 6 shows the graph of $(\alpha h\nu)^2$ vs. photon energy $h\nu$ for the ZnO films deposited at various deposition times.

The estimated band gap values E_g are in good agreement with those published by different authors for ZnO films deposited with sputtering, and are close to the reported one for the single crystal form [23]. E_g decreases with increasing deposition time from 3.39 to 3.28 eV. This is due to the increase of defects or deviation from stoichiometry. The observed blue shift in the band gap energy in these films can also be due to the quantum confinement effect. Indeed, it is well-known that the energy band gap of a semiconductor is affected by the residual strain, defects, charged impurities, disorder at the grain boundaries [24], and also particle confinement. If the films have less thickness and a smaller grain size, the widening of the respective conduction and valence bands will be less, and this results in a wider energy gap [25].

Meanwhile, the band gap values increases from 3.32 to 3.36 eV with an argon pressure increase. The widening of the band gap with an increase of the sputtering pressure might be due to an increase of the carrier density in addition to the Moss-Burstein shift [26]. Such a widening of the band gap was also noticed earlier in nonstoichiometric ZnO films [27].

Evaluation of the refractive indices of optical materials is considerably important for the applications in integrated optics devices, such as switches, filters, and modulation, in which the refractive index is a key parameter for the device design. The refractive indices are affected by crystallinity, electronic structure, and lattice point defects [28].

The refractive index of the deposited films increases slightly with time deposition from 1.93 to 1.96, approaching the refractive index of bulk ZnO, which may be attributed to the improvement in crystallinity.

Meanwhile, the refractive index decreases with argon pressure from 2.28 to 1.93. Such a decrease of the refractive index was also noticed earlier in nonstoichiometric ZnO films deposited with different argon pressures [25].

Film thickness, estimated by the Swanpoel method [29], was in the range of 269 to 371 nm.

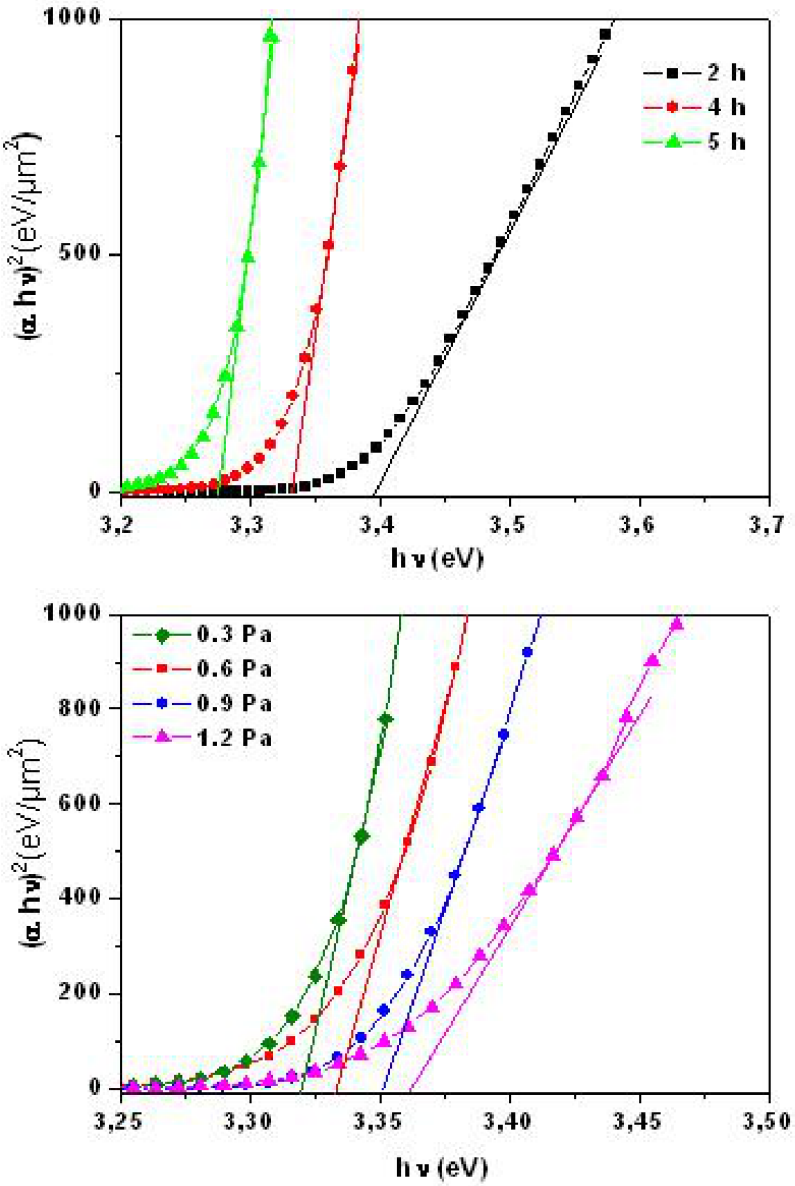

FIG. 6: $(\alpha h\nu)^2$ vs. $h\nu$ plots for ZnO films deposited with (a) different deposition time, and (b) different argon pressures.

III-4. Electrical properties

Impedance measurements were performed with the HP 4192A impedance analyzer in the measurable impedance range from 5 Hz to 13 MHz with data taken at 20 points per decade. Real and imaginary parts of the impedance as a function of frequency were measured and displayed in the complex plane.

Data were taken and treated using a custom HPVee program. Fitting of the data were undertaken with an Ec-Lab program.

Nyquist plots of the ZnO films grown with sputtering using a powder target showed arcs of semicircles or intertwined arcs of semicircles (see Fig. 7).

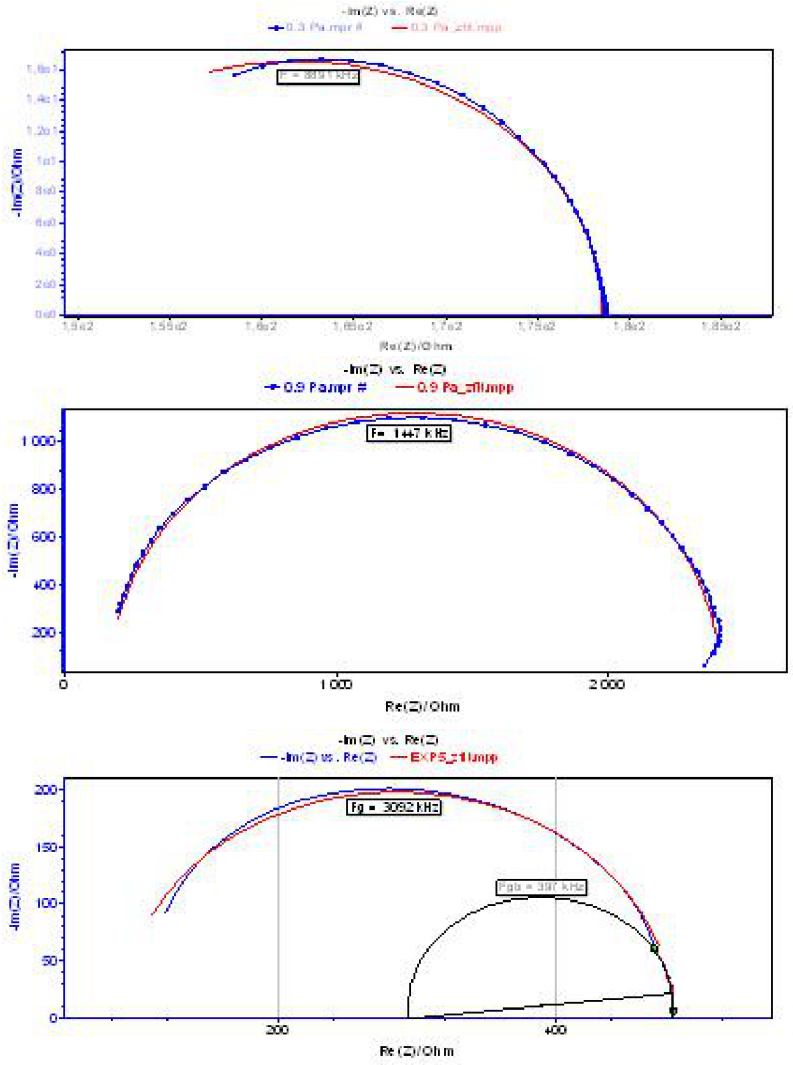

FIG. 7: Nyquist plots for ZnO films deposited with different deposition time, argon pressures of (a) 0.3 Pa, (b) 0.9 Pa, and (c) 1.2 Pa.

Some observed complex impedance spectra show a single semi-circlar arc (Fig. 7a and 7.b). The frequency of relaxation appears at a high frequency (1 to 9 MHz) and indicates that the electric transport mechanism is relative to the grains. The presence of a single arc for each film implies the behavior of a simple parallel RC component.

For the films deposited at an argon pressure of 1.2 Pa (Fig. 7.c), we notice the presence of two semi-circular arcs indicating the presence of two relaxation mechanisms. The first relaxation frequency of about 400 kHz is relative to the electron transport within the grain boundaries, and the second relaxation frequency is relative to the grains of about 3.1 MHz. Two sets of parallel RC components in series can be employed to model the Nyquist plot. The assignment of the grain and grain boundary contributions is consistent with the "brick-layer" model [30], proposed to correlate between the polycrystalline materials' microstructure and their electrical properties.

Knowing the thickness of the samples, the resistivity of the films can be calculated from the total resistance. The lowest resistivity of the ZnO films was about 6.8×10^{-3} Ω.cm obtained at optimum conditions of 0.3 Pa argon pressure and 4 hours deposition time.

Resistivity of the ZnO films grown with sputtering using a powder target have a good resistivity varying from 7×10^{-3} to 8×10^{-2} Ω.cm, although they didn't have a doping or a post deposition treatment.

IV. CONCLUSION

In this study, we successfully prepared ZnO thin films by RF magnetron sputtering using a ZnO powder target. Good quality transparent conducting nanocrystalline undoped zinc oxide films were deposited using this low cost technique.

The X-ray diffraction (XRD) data confirmed the deposition of highly c-axis-oriented (002) ZnO films, and indicated that the crystallinity of the films is improved by increased deposition time and argon pressure. The average size of the crystallites calculated from the XRD patterns of all the films suggests the nanostructured nature of the films. The high transmittance shown by these films is an indication of the enhanced crystalline structure and the very good optical quality. The ZnO film's optical band gap is large and varies between 3.39 and 3.28 eV, a feature of transparent conducting materials. The obtained energy gap results make ZnO film as a promising semiconductor material for solar cell fabrication due to its suitable optical properties.

Under optimum parameters, a resistivity as low as 6.8×10^{-3} Ω·cm and a transmittance of about 85% of ZnO films have been obtained.

References

[1] Y.-J. Kang *et al.*, Sol. Energ. Mat. Sol. Cells **96**, 137 (2012).
[2] H. Kima *et al.*, Thin Solid Films **377-378**, 798 (2000).
[3] K. Ramamoorthy, M. Arivanandhan, K. Sankaranarayanan, and C. Sanjeeviraja, Mater. Chem. Phys. **85**, 257 (2–3) (2004). doi: 10.1016/j.matchemphys.2003.09.018
[4] D.-T. Phan, G.-S. Chung, Appl. Surf. Sci. **257**(9), 4339 (2011).
[5] T. Ates, C. Tatar, F. Yakuphanoglu, Sensor. Actuat. A: Phys. **190**, 153 (2013). doi: 10.1016/j.sna.2012.11.031
[6] F. Chaabouni, M. Abaab, B. Rezig, Sensor. Actuat. B **100**, 200 (2004).

doi: 10.1016/j.snb.2003.12.059
[7] D. Spemann, E. M. Kaidashev, M. Lorenz, J. Vogt, and T. Butz, Nuc. Instr. Meth. Phys. Res. B **219-220**, 891 (2004).
[8] H. Czternastek, A. Brudnik, M. Jachimowski, and E. Kolawa, J. Phys. D: Appl. Phys. **25**, 865 (1992). doi: 10.1088/0022-3727/25/5/019
[9] J. Löffler, R. Groenen, J. L. Linden, M. C. M. van de Sanden, and R. E. I. Schropp, Thin Solid Films **392** (2), 315 (2001). doi: 10.1016/S0040-6090(01)01050-1
[10] K. Sakurai *et al.*, J. Cryst. Growth **214**–**215**, 92 (2000).
[11] M. Audronis, P. J. Kelly, R. D. Arnell, A. Leyland, and A. Matthews, Surf. Coat. Tech. **200**, 1366 (2005). doi: 10.1016/j.surfcoat.2005.08.022
[12] Y. Zhou, P. J. Kelly, A. Postill, O. Abu-Zeid, and A. A. Alnajjar, Thin Solid Films **447**–**448**, 33 (2004).
[13] J. G. E. Gardeniers, Z. M. Rittersma, and G. J. Burger, J. Appl. Phys. **83**, 7844 (1998). doi: 10.1063/1.367959
[14] G. Knuyt, C. Quaeyhagens, J. D. Haen, and L. M. Stals, Thin Solid Films **258**, 159 (1995). doi: 10.1016/0040-6090(94)06353-2
[15] D. Cullity, *Elements of X-Ray Diffraction*, 2nd ed. (Addison-Wesley, Reading, 1978), p. 68.
[16] J. F. Chang, H. L. Wang, and M. H. Hon, J. Cryst. Growth **211**, 93 (2000). doi: 10.1016/S0022-0248(99)00779-4
[17] A. Segmuller and M. Murakami, in *Analytical Techniques for Thin Films*, eds. K. N. Tu and R. Rosenberg (Academic Press, Boston, 1988), p. 143.
[18] Q. Zhenxing, Z. Xiaozhong, Z. Mingzhou, W. Xizhang, and L. Yujin, IEEE Trans. Sonics Ultrason. SU- **32** (5), 630 (1985).
[19] T. B. Bateman, Appl. Phys. **33**, 3309 (1962). doi: 10.1063/1.1931160
[20] J. A. Thornton and D. W. Hoffman, Thin Solid Films **171**, 5 (1989). doi: 0.1016/0040-6090(89)90030-8
[21] J. Hinze and K. Ellmer, J. Appl. Phys. **88**, 2443 (2000). doi: 10.1063/1.1288162
[22] F. Abélès, in Optical properties of solids, (ed. F. Abelès: North-Holland Publication, Amsterdam, 1972), p.303
[23] S. Major, A. Banerjee, and K. L. Chopra, Thin Solid Films **108**, 333 (1983). doi: 10.1016/0040-6090(83)90082-2
[24] J. D. Dow and D. Redfield, Phys. Rev. B **5**, 594 (1972). doi: 10.1103/PhysRevB.5.594
[25] I. P. Batra, P. Wurfel, and B. D. Silverman, Phys. Rev. Lett. **30**, 384 (1973). doi: 10.1103/PhysRevLett.30.384
[26] T. S. Moss, Phys. Soc. Lond. B **67**, 775 (1954).
[27] A. P. Roth, J. B. Webb, and D. F. Williams, Phys. Rev. B: Condens. Mat. Mat. Phys. **25**, 7836 (1982). doi: 10.1103/PhysRevB.25.7836
[28] C. J. Lu, S. B. Ren, H. M. Shen, J. S. Liu, and Y. N. Wang, J. Vac. Sci. Technol. A **15**, 2167 (1997).
[29] R. Swanpoel, J. Phys. E **16**, 1214 (1983). doi: 10.1088/0022-3735/16/12/023
[30] J. R. Macdonald, *Impedance Spectroscopy Emphasizing Solid Materials and System*, (Wiley, New York, 1987), p. 40.